Electronic Supplementary Material (ESI) for Dalton Transactions.

SUPPORTING INFORMATION

A family of carboxylate-diphenoxo triply bridged dimetallic $Zn^{II}Ln^{III}$ complexes: SMM behavior and luminescent properties

Itziar Oyarzabal, Beñat Artetxe, Antonio Rodríguez-Diéguez, José Ángel García, José Manuel Seco and Enrique Colacio

Index:

1. Elemental Analyses and Crystallographic Tables.

Table S1.- Yields and elemental analyses for complexes **1-11**

Complex	Yield (%)	Formula	% C calc./found	% H calc./found	% N calc./found
1	69	$C_{24}H_{26}N_5O_{12}Br_2ZnPr$	30.58/30.64	2.78/2.81	7.43/7.47
2	71	$C_{24}H_{26}N_5O_{12}Br_2ZnNd$	30.47/30.52	2.77/2.79	7.40/7.42
3	65	$C_{24}H_{26}N_5O_{12}Br_2ZnSm$	30.28/30.35	2.75/2.76	7.36/7.39
4	60	$C_{24}H_{26}N_5O_{12}Br_2ZnEu$	30.23/30.25	2.75/2.78	7.34/7.38
5	63	$C_{24}H_{26}N_5O_{12}Br_2ZnGd$	30.06/30.13	2.73/2.75	7.30/7.35
6	62	$C_{24}H_{26}N_5O_{12}Br_2ZnTb$	30.01/30.09	2.73/2.75	7.29/7.34
7	68	$C_{24}H_{26}N_5O_{12}Br_2ZnDy$	29.90/29.94	2.72/2.76	7.26/7.30
8	61	$C_{24}H_{26}N_5O_{12}Br_2ZnHo$	29.82/29.88	2.71/2.73	7.24/7.28
9	70	$C_{24}H_{26}N_5O_{12}Br_2ZnEr$	29.75/29.83	2.71/2.75	7.23/7.30
10	58	$C_{24}H_{26}N_5O_{12}Br_2ZnTm$	29.70/29.72	2.70/2.71	7.22/7.25
11	63	$C_{24}H_{26}N_5O_{12}Br_2ZnYb$	29.57/29.61	2.69/2.70	7.18/7.21

Table S2.- Crystallographic data for compounds **1**, **2** and **4**-**6**.

Compound	**1**	**2**	**4**	**5**	**6**
Formula	$C_{24}H_{26}N_5O_{12}Br_2ZnPr$	$C_{24}H_{26}N_5O_{12}Br_2ZnNd$	$C_{24}H_{26}N_5O_{12}Br_2ZnEu$	$C_{24}H_{26}N_5O_{12}Br_2ZnGd$	$C_{24}H_{26}N_5O_{12}Br_2ZnTb$
M_r	942.60	945.93	953.65	958.94	960.61
Crystal system	Monoclinic	Monoclinic	Monoclinic	Monoclinic	Monoclinic
Space group (no.)	*P21/n* (14)	*P21/n* (14)	*P21/n* (14)	*P21/n* (14)	*P21/n* (14)
a (Å)	13.45653(19)	13.4135(2)	13.5257(2)	13.4496(5)	13.5017(6)
b (Å)	14.75424(18)	14.7713(2)	14.9372(2)	14.7776(5)	14.7618(4)
c (Å)	16.2850(3)	16.1930(2)	15.8049(2)	16.0073(6)	15.9579(6)
α (°)	90	90	90	90	90
β (°)	91.4469(14)	91.2300(10)	90.109(2)	91.051(3)	91.315(4)
γ (°)	90	90	90	90	90
V (Å^3)	3232.21(8)	3207.66(8)	3193.15(8)	3181.0(2)	3179.7(2)
Z	4	4	4	4	4
D_c (g cm^{-3})	1.937	1.959	1.984	2.002	2.007
μ(MoKα) (mm^{-1})[d]	4.770	4.906	18.361	5.400	5.540
*T (*K)	100(2)	100(2)	100(2)	100(2)	100(2)
Observed reflections	6350 (5141)	5633 (4984)	6406 (6158)	5574 (4651)	6584 (5277)
R_{int}	0.0306	0.0293	0.0308	0.0392	0.0462
Parameters	410	410	409	410	410
*G*OF	1.013	1.126	1.036	1.076	1.064
R_1[a,b]	0.0484 (0.0343)	0.0301 (0.0248)	0.0302 (0.0288)	0.0492 (0.0375)	0.0529 (0.0368)
wR_2[c]	0.0697 (0.0642)	0.0680 (0.0654)	0.0818 (0.0805)	0.0989 (0.0930)	0.0875 (0.0807)
Largest difference in peak and hole (e Å^{-3})	1.180 and -0.724	2.035 and -0.478	2.441 and -0.874	2.148 and -1.013	1.903 and -0.888

[a] $R_1 = \Sigma||F_o| - |F_c||/\Sigma|F_o|$. [b] Values in parentheses for reflections with $I > 2\sigma(I)$. [c] $wR_2 = \{\Sigma[w(Fo^2 - Fc^2)^2] / \Sigma[w(Fo^2)^2]\}^{½}$ [d] μ(CuKα) (mm^{-1}) in **4**

Table S3.- Crystallographic data for compounds **7** and **9**-**11**.

Compound	**7**	**9**	**10**	**11**
Formula	$C_{24}H_{26}N_5O_{12}Br_2ZnDy$	$C_{24}H_{26}N_5O_{12}Br_2ZnEr$	$C_{24}H_{26}N_5O_{12}Br_2ZnTm$	$C_{24}H_{26}N_5O_{12}Br_2ZnYb$
M_r	964.19	968.95	970.62	974.73
Crystal system	Monoclinic	Monoclinic	Monoclinic	Monoclinic
Space group (no.)	*P21/n* (14)	*P21/n* (14)	*P21/n* (14)	*P21/n* (14)
a (Å)	13.5589(12)	13.5236(2)	13.5836(6)	13.5447(10)
b (Å)	14.8592(11)	14.7278(17)	14.8415(5)	14.8034(12)
c (Å)	15.8350(12)	15.9106(2)	15.6820(6)	15.7092(11)
α (°)	90	90	90	90
β (°)	90.618(3)	91.294(2)	90.237(3)	90.5320(10)
γ (°)	90	90	90	90
V (Å^3)	3190.2(4)	3168.2(4)	3161.5(2)	3149.7(4)
Z	4	4	4	4
D_c (g cm^{-3})	2.008	2.031	2.039	2.056
μ(MoKα) (mm^{-1})[d]	5.647	5.977	6.141	9.852
T (K)	100(2)	100(2)	100(2)	100(2)
Observed reflections	5617 (4883)	5571 (4995)	6540 (5821)	6446 (6158)
R_{int}	0.0426	0.0277	0.0328	0.0236
Parameters	410	410	410	410
*G*OF	1.080	1.065	1.038	1.088
R_1[a,b]	0.0363 (0.0289)	0.0295 (0.0242)	0.0288 (0.0237)	0.0261 (0.0246)
wR_2[c]	0.0786 (0.0750)	0.0611 (0.0583)	0.0505 (0.0489)	0.0636 (0.0627)
Largest difference in peak and hole (e Å^{-3})	2.851 and -0.398	1.834 and -0.563	0.921 and -0.811	0.848 and -1.138

[a] $R_1 = \Sigma||F_o| - |Fc||/\Sigma|F_o|$. [b] Values in parentheses for reflections with $I > 2\sigma(I)$. [c] $wR_2 = \{\Sigma[w(Fo^2 - Fc^2)^2] / \Sigma[w(Fo^2)^2]\}^{½}$ [d] μ(CuKα) (mm^{-1}) in **11**

Table S4.- Bond lengths (Å) and angles (°) for compounds **1**, **2** and **4**-**6**.

Compound	**1**	**2**	**4**	**5**	**6**
Ln(1)···Zn(1)	3.437(1)	3.426(1)	3.406(1)	3.399(1)	3.383(1)
Ln(1)-O(1A)	2.432(3)	2.421(2)	2.384(2)	2.364(4)	2.355(3)
Ln(1)-O(2A)	2.471(3)	2.447(2)	2.401(2)	2.401(4)	2.384(3)
Ln(1)-O(3A)	2.424(3)	2.407(2)	2.374(2)	2.367(4)	2.354(3)
Ln(1)-O(4A)	2.454(3)	2.443(2)	2.400(3)	2.380(4)	2.373(4)
Ln(1)-O(2P)bridge	2.393(3)	2.382(2)	2.337(2)	2.318(4)	2.312(4)
Ln(1)-O(1C)nitrate	2.573(3)	2.551(2)	2.486(2)	2.509(4)	2.472(4)
Ln(1)-O(2C)nitrate	2.545(3)	2.536(3)	2.532(2)	2.472(4)	2.492(4)
Ln(1)-O(1D)nitrate	2.557(3)	2.553(2)	2.518(2)	2.480(4)	2.462(4)
Ln(1)-O(2D)nitrate	2.572(3)	2.534(2)	2.494(3)	2.523(4)	2.518(4)
Zn(1)-N(1A)	2.133(3)	2.132(3)	2.131(3)	2.127(4)	2.130(4)
Zn(1)-N(2A)	2.099(3)	2.096(3)	2.105(3)	2.090(5)	2.103(4)
Zn(1)-O(2A)	2.081(3)	2.083(2)	2.077(2)	2.069(4)	2.072(3)
Zn(1)-O(3A)	2.149(3)	2.146(2)	2.130(2)	2.127(4)	2.127(3)
Zn(1)-O(1P)bridge	1.953(3)	1.955(2)	1.967(2)	1.951(4)	1.952(4)
Ln(1)-O(2A)-Zn(1)	97.70(10)	97.94(8)	98.77(9)	98.72(14)	98.55(13)
Ln(1)-O(3A)-Zn(1)	97.26(11)	97.46(9)	98.12(9)	98.16(15)	97.92(13)
O(2A)-Ln(1)-O(3A)	70.09(9)	70.26(7)	70.18(8)	69.90(12)	70.54(11)
O(2A)-Ln(1)-O(2P)bridge	78.55(10)	78.48(8)	78.76(9)	79.14(13)	79.38(12)
O(3A)-Ln(1)-O(2P)bridge	78.87(10)	78.90(8)	79.50(8)	79.90(13)	80.10(13)
O(2A)-Zn(1)-O(3A)	83.26(11)	82.67(8)	81.45(9)	81.22(14)	81.30(13)
O(2A)-Zn(1)-O(1P)bridge	105.74(12)	105.76(9)	104.73(10)	104.99(16)	104.75(14)
O(3A)-Zn(1)-O(1P)bridge	98.62(12)	98.46(9)	98.79(10)	98.58(15)	98.63(15)

Table S5.- Bond lengths (Å) and angles (°) for compounds **7** and **9-11**.

Compound	**7**	**9**	**10**	**11**
Ln(1)···Zn(1)	3.388(1)	3.371(1)	3.371(1)	3.360(1)
Ln(1)-O(1A)	2.345(3)	2.330(3)	2.314(2)	2.303(2)
Ln(1)-O(2A)	2.380(3)	2.361(2)	2.338(2)	2.336(2)
Ln(1)-O(3A)	2.348(3)	2.325(3)	2.316(2)	2.307(2)
Ln(1)-O(4A)	2.369(3)	2.343(3)	2.327(2)	2.320(2)
Ln(1)-O(2P)bridge	2.285(3)	2.275(3)	2.261(2)	2.241(2)
Ln(1)-O(1C)nitrate	2.484(3)	2.462(3)	2.463(2)	2.459(2)
Ln(1)-O(2C)nitrate	2.450(4)	2.432(3)	2.417(2)	2.409(2)
Ln(1)-O(1D)nitrate	2.511(3)	2.485(3)	2.411(2)	2.406(2)
Ln(1)-O(2D)nitrate	2.449(3)	2.427(3)	2.513(2)	2.501(2)
Zn(1)-N(1A)	2.131(4)	2.133(3)	2.128(2)	2.127(2)
Zn(1)-N(2A)	2.106(4)	2.101(3)	2.108(3)	2.109(2)
Zn(1)-O(2A)	2.076(3)	2.071(3)	2.078(2)	2.075(2)
Zn(1)-O(3A)	2.118(3)	2.114(3)	2.114(2)	2.108(2)
Zn(1)-O(1P)bridge	1.960(3)	1.960(3)	1.966(2)	1.961(2)
Ln(1)-O(2A)-Zn(1)	98.78(12)	98.85(10)	99.33(7)	99.05(8)
Ln(1)-O(3A)-Zn(1)	98.54(12)	98.71(10)	98.97(8)	98.98(8)
O(2A)-Ln(1)-O(3A)	70.24(10)	70.31(9)	70.41(7)	80.78(7)
O(2A)-Ln(1)-O(2P)bridge	79.25(11)	79.71(9)	79.93(7)	80.21(7)
O(3A)-Ln(1)-O(2P)bridge	80.08(11)	80.47(9)	80.62(8)	80.78(7)
O(2A)-Zn(1)-O(3A)	80.84(12)	80.29(10)	79.61(8)	79.81(8)
O(2A)-Zn(1)-O(1P)bridge	104.09(13)	104.28(11)	103.43(8)	103.32(8)
O(3A)-Zn(1)-O(1P)bridge	98.53(13)	98.62(11)	98.68(8)	98.25(8)

2. Experimental XRPD.

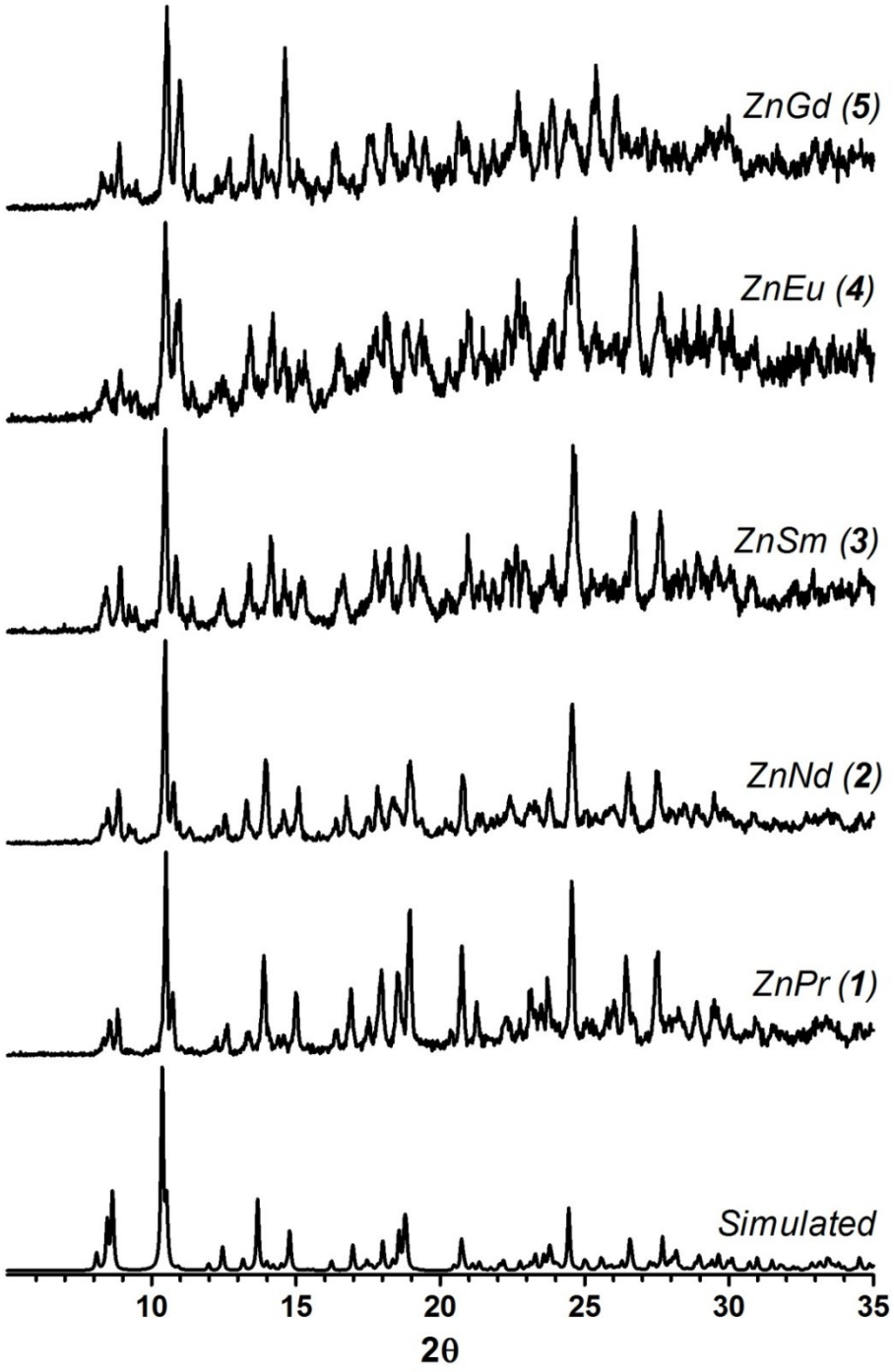

Figure S1.- Experimental XRPD for complexes **1**-**5** together with a simulated pattern of the Nd^{III} complex **2** extracted from single-crystal X-ray diffractions.

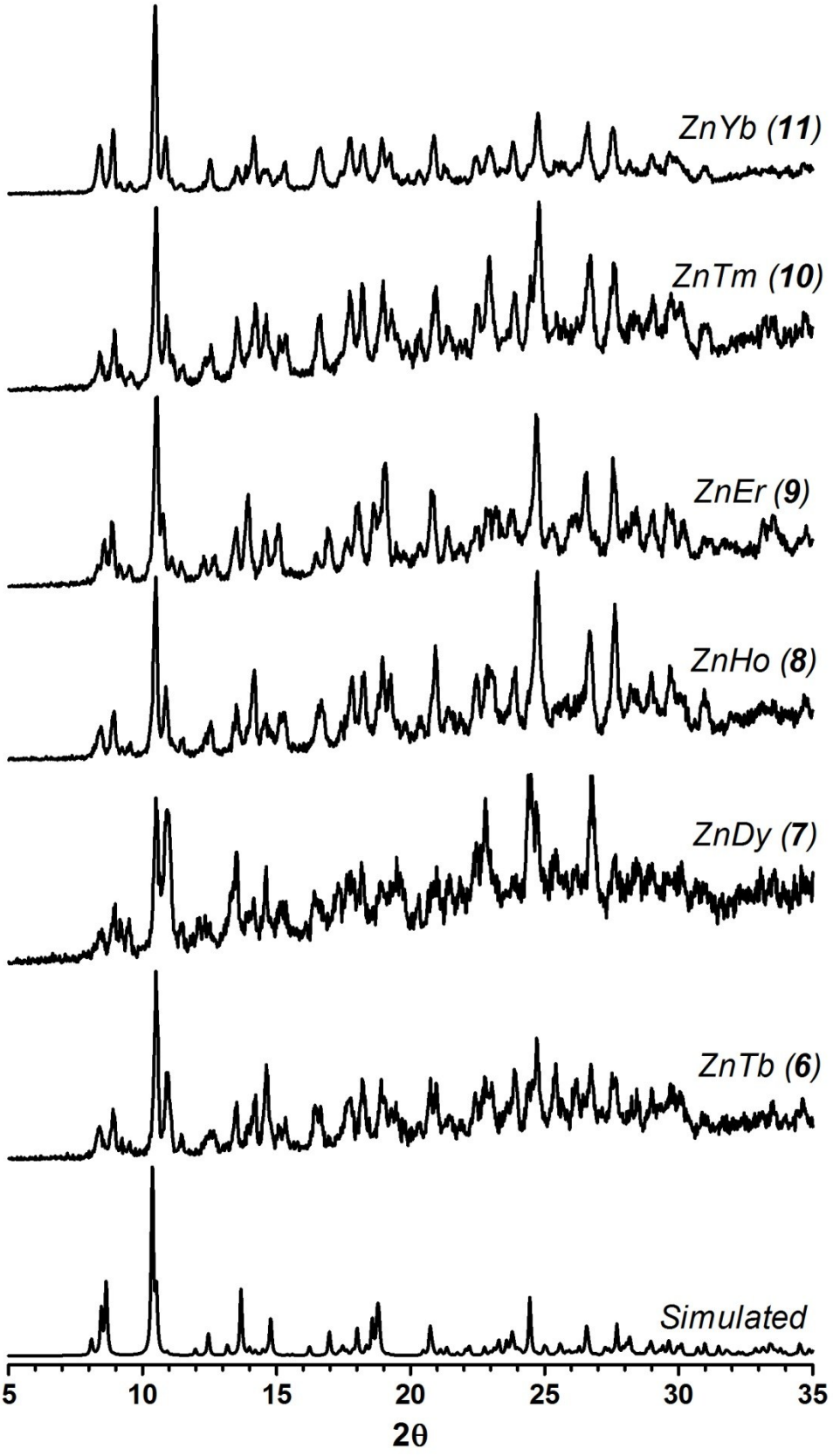

Figure S2.- Experimental XRPD for complexes **6-11** together with a simulated pattern of the Nd^{III} complex **2** extracted from single-crystal X-ray diffractions

3. Continuous Shape Measurements.

Table S6.- Continuous Shape Measurements for the ZnN_2O_3 coordination environment. Low values indicate high proximity to the analyzed ideal geometry.

PP-5 1 D5h Pentagon
vOC-5 2 C4v Vacant octahedron
TBPY-5 3 D3h Trigonal bipyramid
SPY-5 4 C4v Spherical square pyramid
JTBPY-5 5 D3h Johnson trigonal bipyramid J12

	PP-5	**vOC-5**	**TBPY-5**	**SPY-5**	**JTBPY-5**
Comp 1	32.271	1.845	3.42	0.463	5.599
Comp 2	32.26	1.928	3.395	0.481	5.617
Comp 4	31.726	2.13	3.387	0.528	5.748
Comp 5	31.847	2.056	3.44	0.522	5.71
Comp 6	31.629	2.1	3.35	0.557	5.659
Comp 7	31.524	2.212	3.333	0.597	5.722
Comp 9	31.425	2.237	3.326	0.618	5.694
Comp 10	31.071	2.361	3.35	0.671	5.803
Comp 11	31.21	2.349	3.32	0.687	5.771

Table S7.- Continuous Shape Measurements for the LnO_9 coordination environment. Low values indicate high proximity to the analyzed ideal geometry.

EP-9 1 D9h Enneagon
OPY-9 2 C8v Octagonal pyramid
HBPY-9 3 D7h Heptagonal bipyramid
JTC-9 4 C3v Johnson triangular cupola J3
JCCU-9 5 C4v Capped cube J8
CCU-9 6 C4v Spherical-relaxed capped cube
JCSAPR-9 7 C4v Capped square antiprism J10
CSAPR-9 8 C4v Spherical capped square antiprism
JTCTPR-9 9 D3h Tricapped trigonal prism J51
TCTPR-9 10 D3h Spherical tricapped trigonal prism
JTDIC-9 11 C3v Tridiminished icosahedron J63
HH-9 12 C2v Hula-hoop
MFF-9 13 Cs Muffin

	EP-9	OPY-9	HBPY-9	JTC-9	JCCU-9	CCU-9	JCSAPR-9	CSAPR-9	JTCTPR-9	TCTPR-9	JTDIC-9	HH-9	MFF-9
Comp 1	34.971	23.365	18.989	15.234	10.202	8.99	2.243	1.412	3.483	2.035	11.066	10.910	1.567
Comp 2	34.999	23.173	19.08	15.231	10.15	9.07	2.197	1.365	3.440	1.971	11.131	11.081	1.538
Comp 4	34.634	22.974	19.138	14.867	9.838	8.928	2.092	1.319	3.127	1.793	11.632	11.518	1.531
Comp 5	34.833	23.164	19.211	15.148	9.878	9.017	1.942	1.206	3.169	1.856	11.552	11.511	1.454
Comp 6	34.921	23.156	19.217	15.211	9.855	9.015	1.874	1.156	3.141	1.827	11.700	11.638	1.421
Comp 7	34.693	23.12	19.316	14.99	9.804	8.974	1.893	1.18	3.041	1.772	11.908	11.768	1.452
Comp 9	34.955	23.226	19.269	15.271	9.819	9.009	1.747	1.045	3.065	1.780	11.967	11.855	1.341
Comp 10	34.629	23.111	19.332	14.966	9.658	8.931	1.748	1.124	2.859	1.721	12.147	11.998	1.422
Comp 11	34.637	23.101	19.32	14.962	9.657	8.951	1.703	1.094	2.829	1.708	12.199	12.076	1.407

4. Magnetic Measurements.

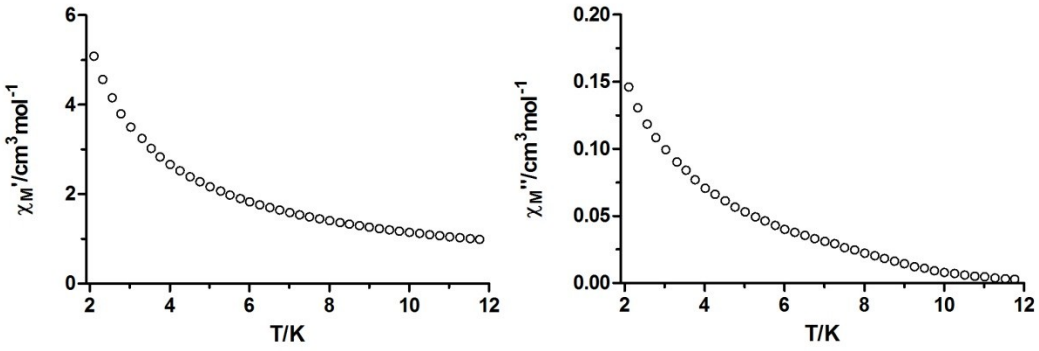

Figure S3.- Temperature dependence of in-phase χ_M' (left) and out-of-phase χ_M'' (right) components of the *ac* susceptibility for complex **7** measured under zero applied *dc* field.

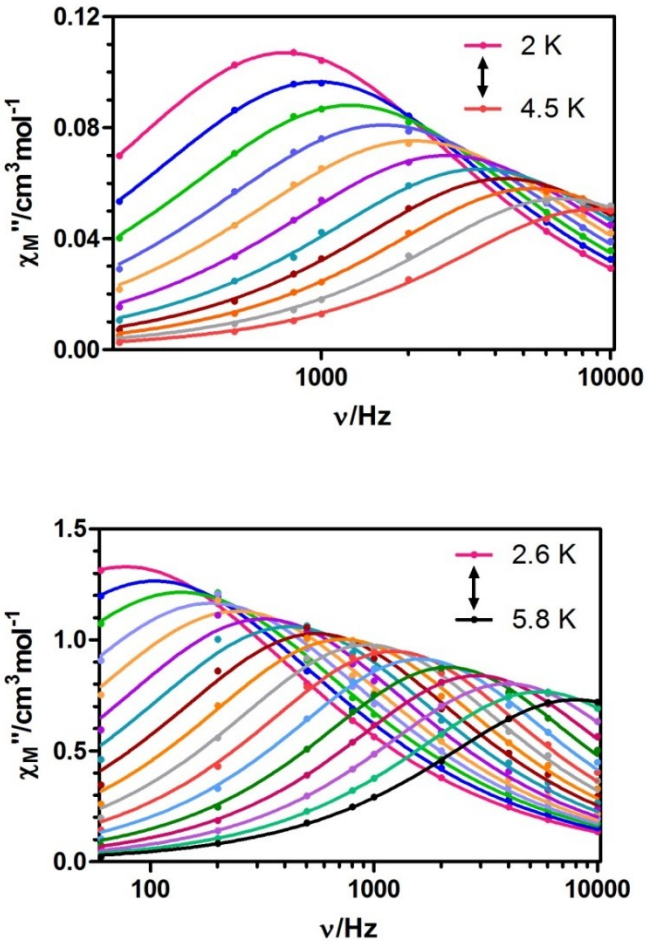

Figure S4.- Variable-temperature frequency dependence of the χ_M'' signal under 1000 Oe applied field for **2** (top) and **7** (bottom). Solid lines represent the best fitting of the experimental data to the Debye model.

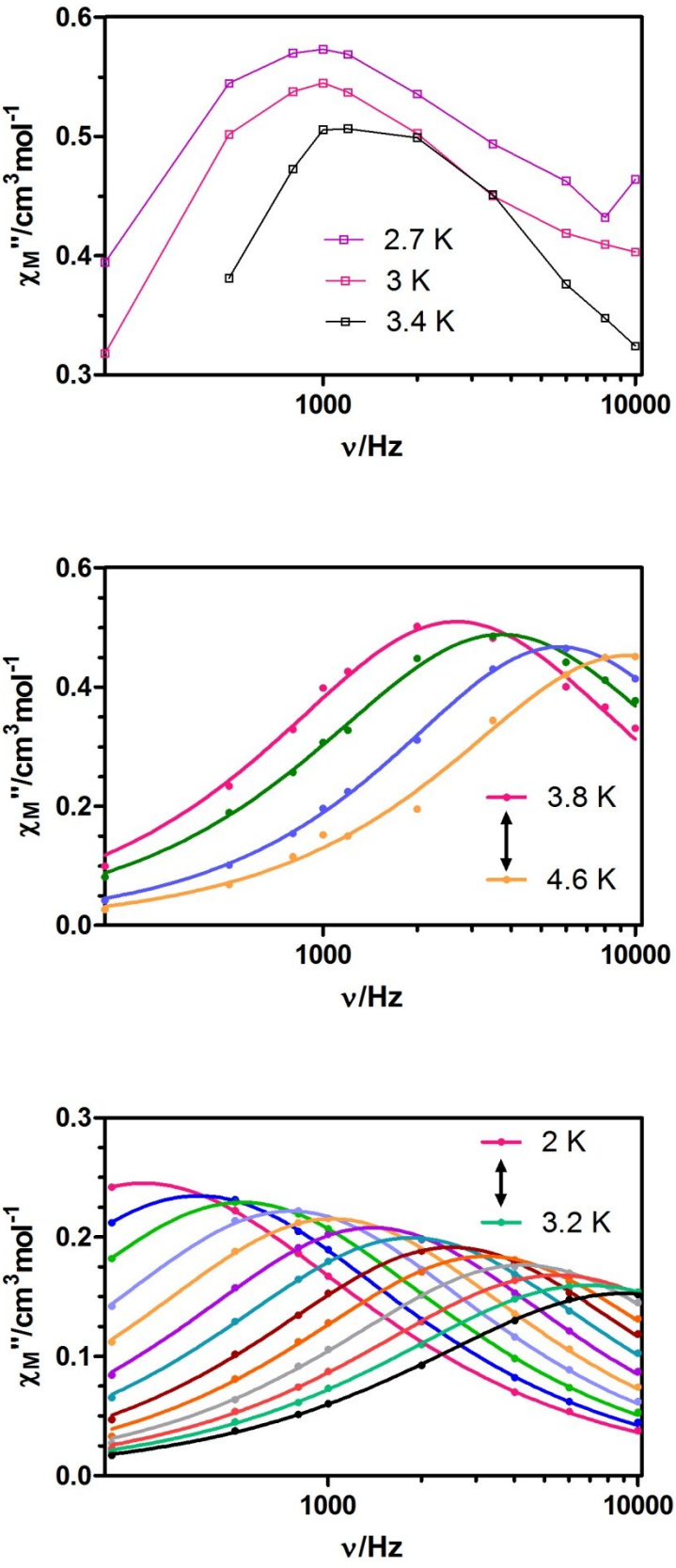

Figure S5.- Variable-temperature frequency dependence of the χ_M'' signal under 1000 Oe applied field for **9** (top and middle) and **11** (bottom). Solid lines are a guide to the eye in the upper plot, while in the two lower plots the lines represent the best fitting of the experimental data to the Debye model.

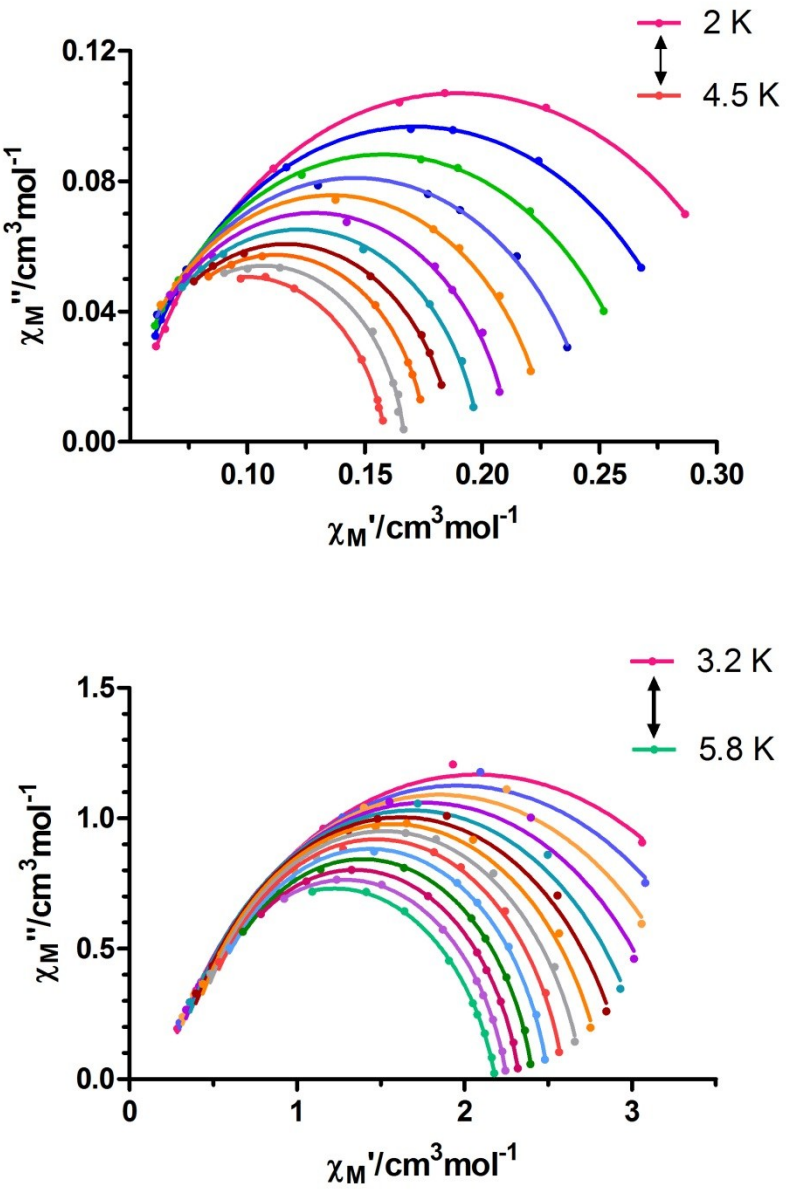

Figure S6.- Cole-Cole plot under 1000 Oe field for **2** (top) and **7** (bottom). Solid lines represent the best fits to the generalized Debye model.

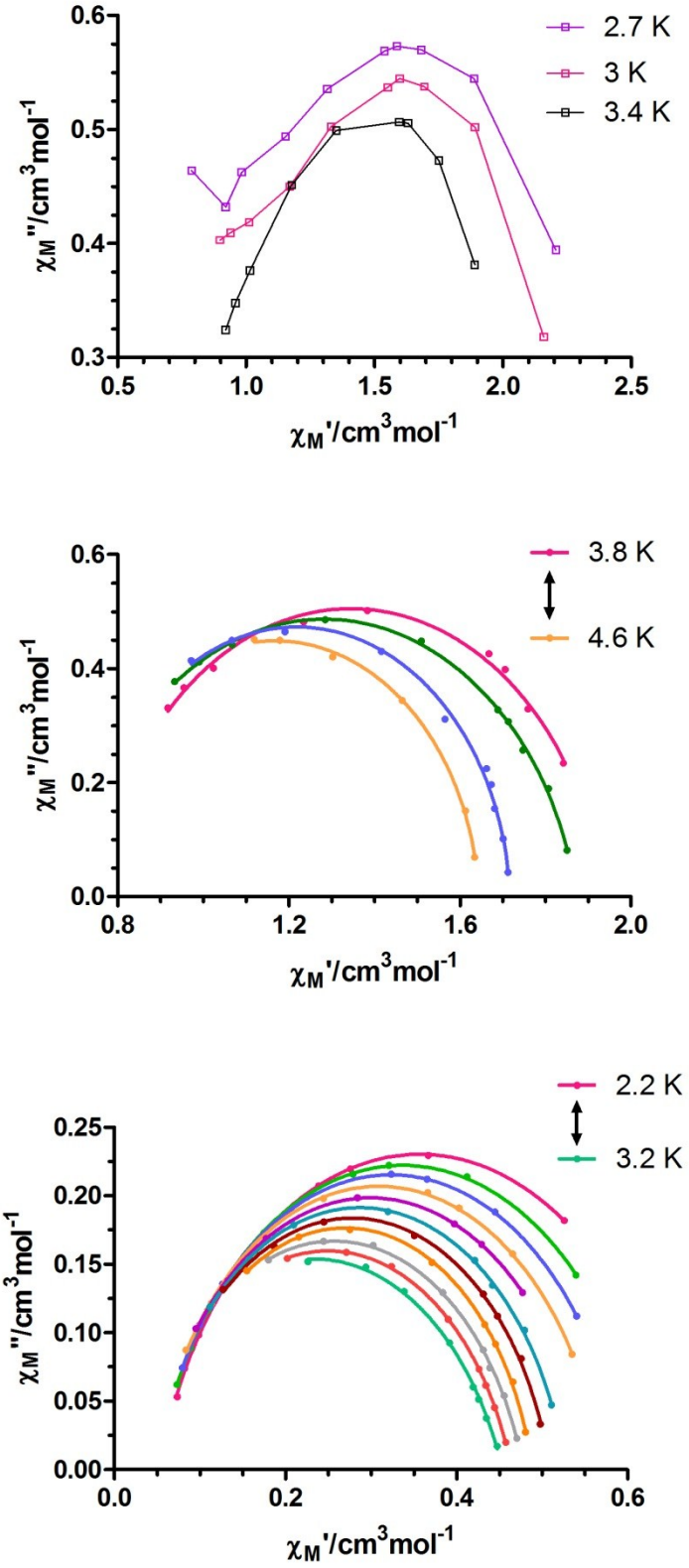

Figure S7.- Cole-Cole plot under 1000 Oe field for **9** (top and middle) and **11** (bottom). Solid lines are a guide to the eye in the upper plot, while in the two lower plots the lines represent the best fitting of the experimental data to the Debye model.

5. Reflectance Spectra.

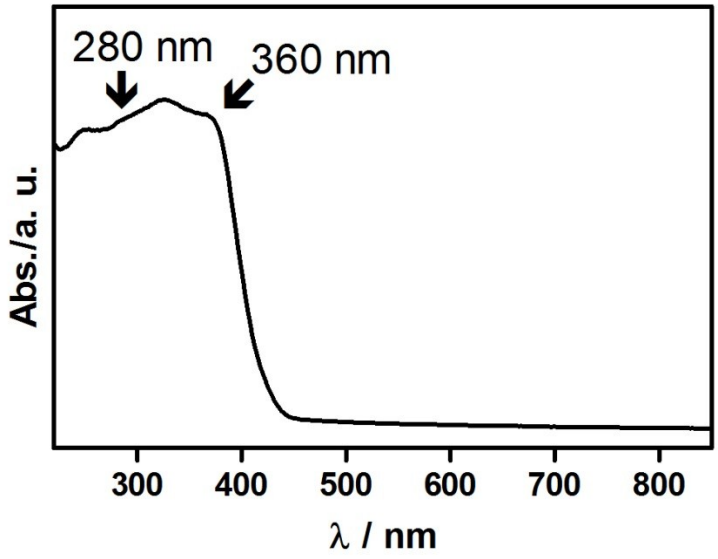

Figure S8.- Reflectance spectrum of the ligand.

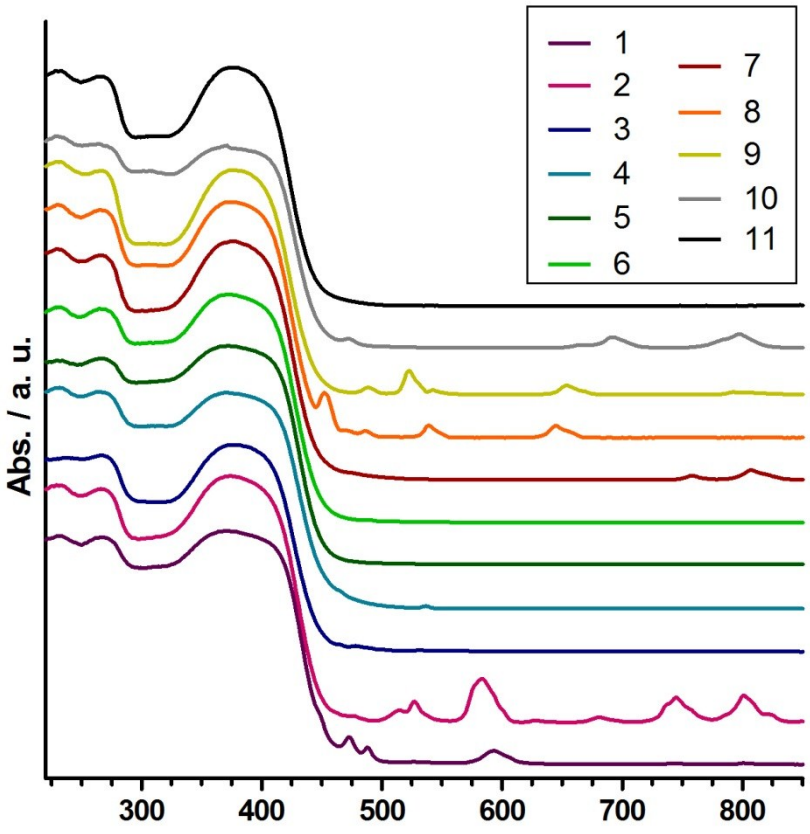

Figure S9.- Reflectance spectra of compounds **1-11**.

6. Luminescence Properties.

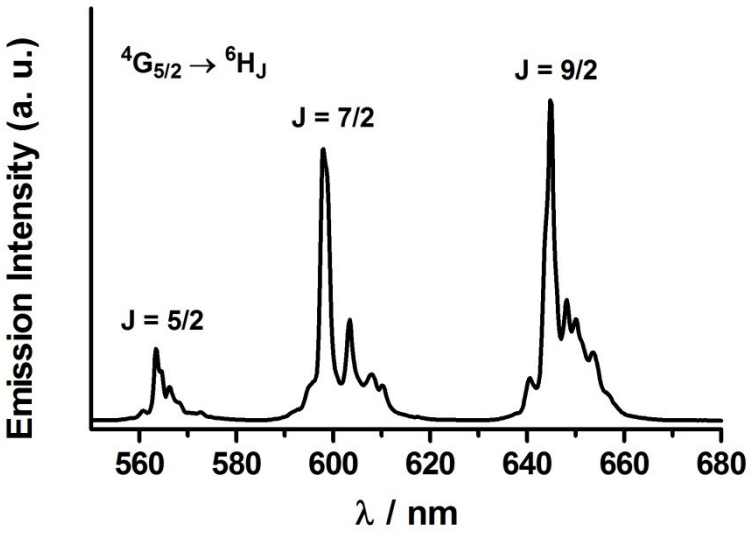

Figure S10.- Solid state photoluminescence spectra for Sm^{III} compound **3** recorded at 10 K upon excitation at 375 nm.

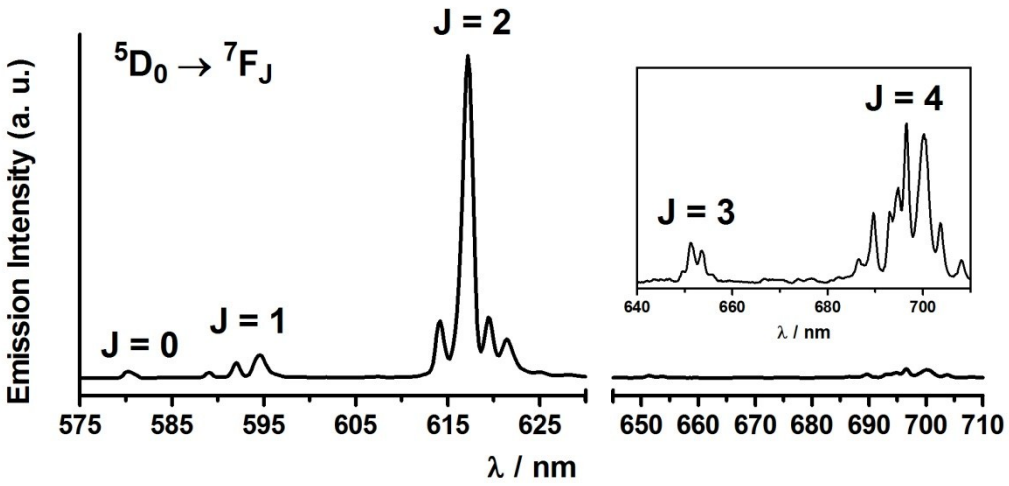

Figure S11.- Solid state photoluminescence spectra for Eu^{III} compound **4** recorded at 10 K upon excitation at 375 nm. The inset shows a detailed view of the less intense transition bands.

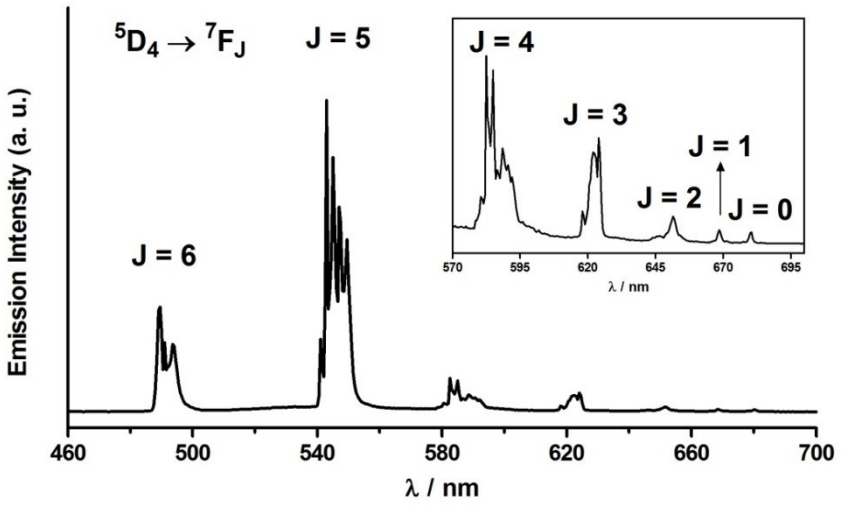

Figure S12.- Solid state photoluminescence spectra for Tb^{III} compound **6** recorded at 10 K upon excitation at 375 nm. The inset shows a detailed view of the less intense transition bands.

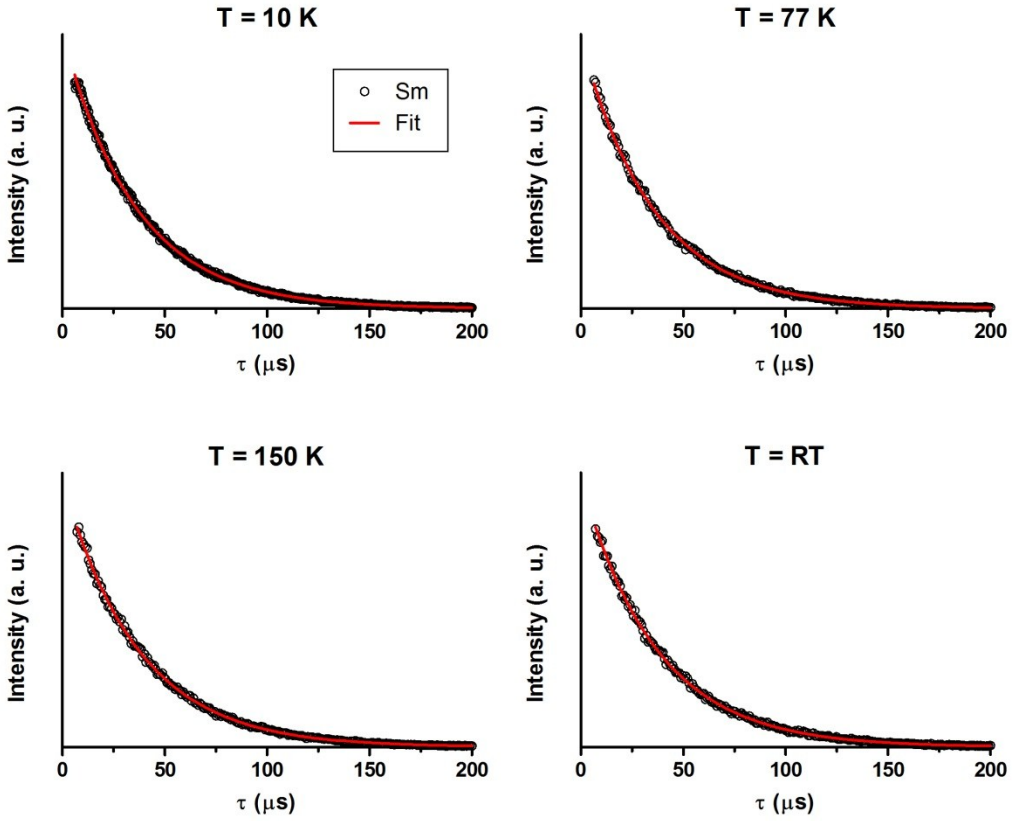

Figure S13.- Luminescence decay curves at different temperatures after excitation at 280 nm for Sm^{III} compound **3** monitored at 645 nm.

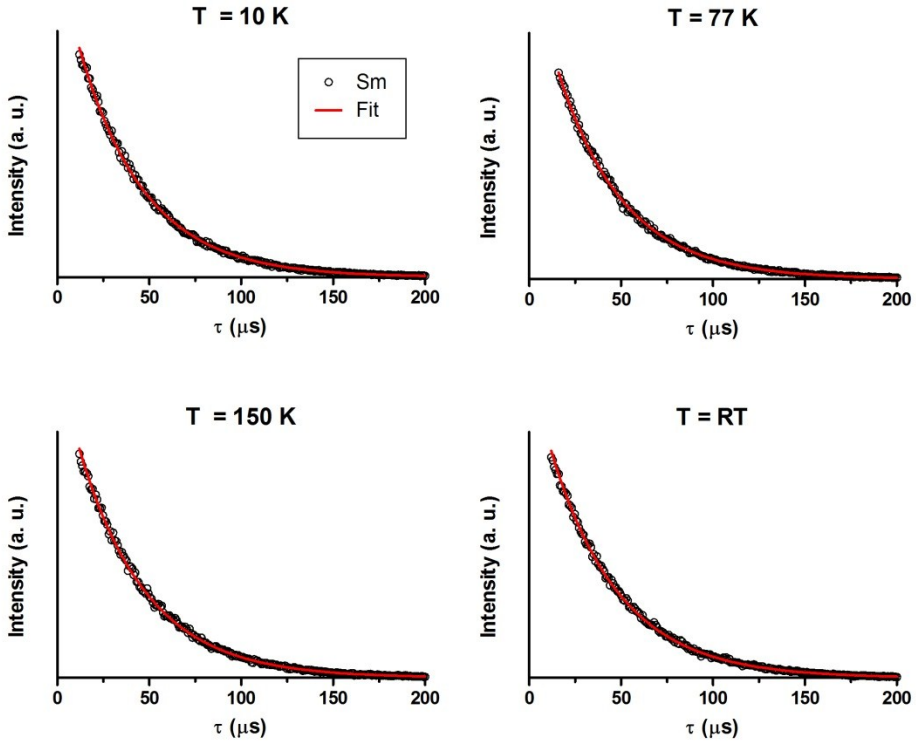

Figure S14.- Luminescence decay curves at different temperatures after excitation at 375 nm for Sm^{III} compound **3** monitored at 645 nm.

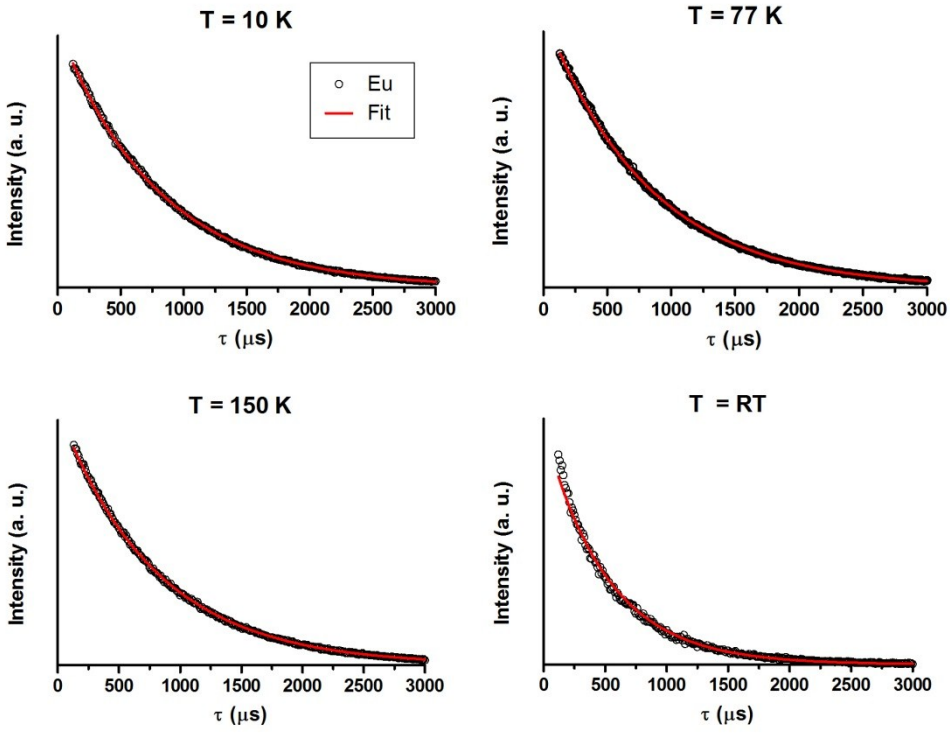

Figure S15.- Luminescence decay curves at different temperatures after excitation at 280 nm for Eu^{III} compound **4** monitored at 617 nm.

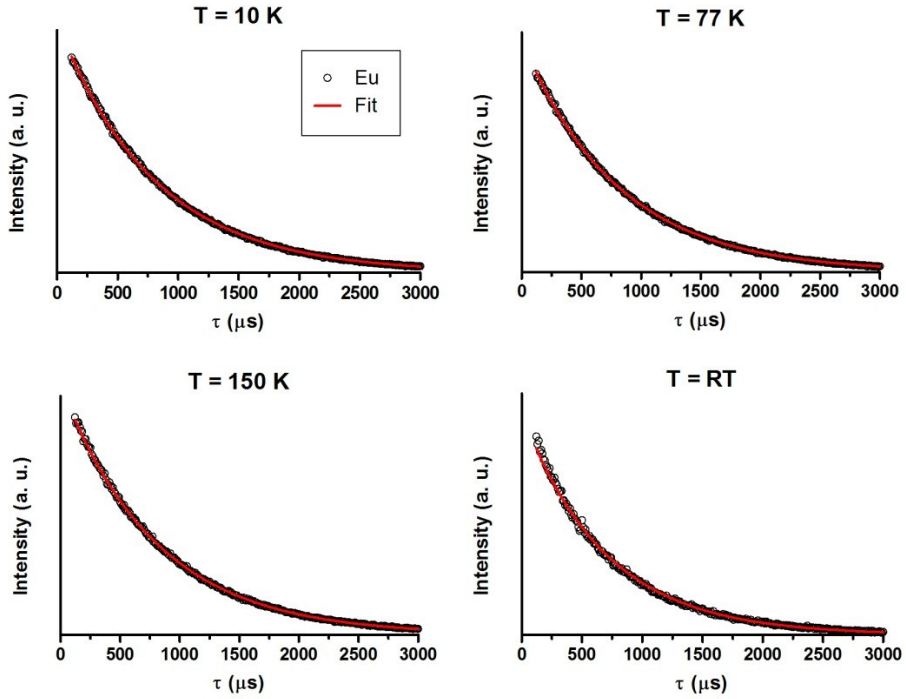

Figure S16.- Luminescence decay curves at different temperatures after excitation at 375 nm for Eu^{III} compound **4** monitored at 617 nm.

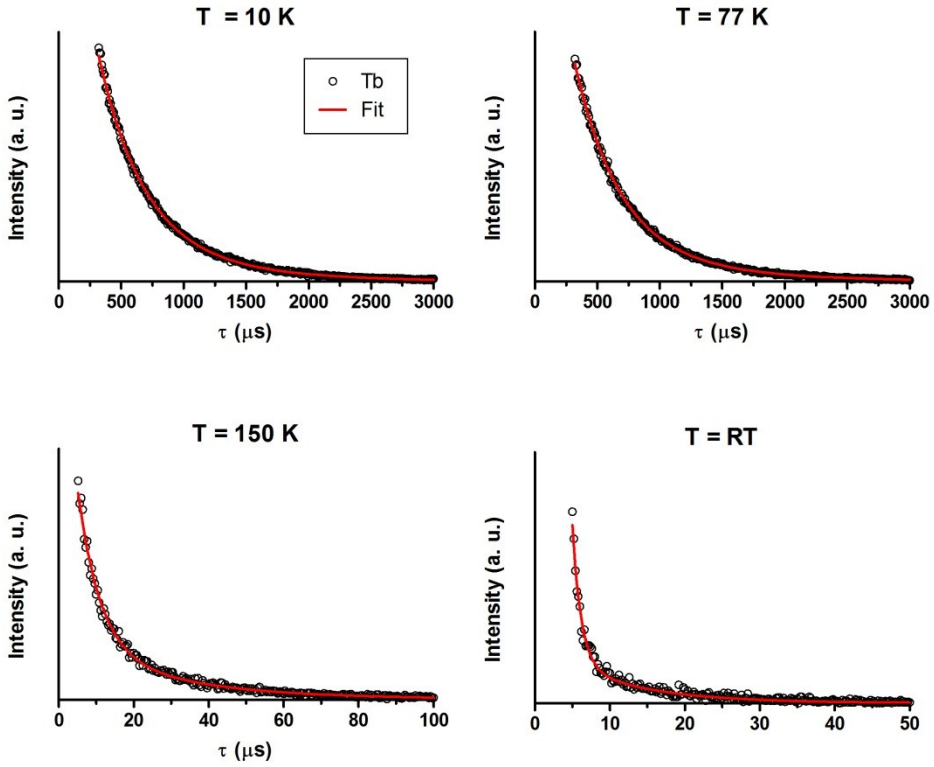

Figure S17.- Luminescence decay curves at different temperatures after excitation at 280 nm for Tb^{III} compound **6** monitored at 545 nm.

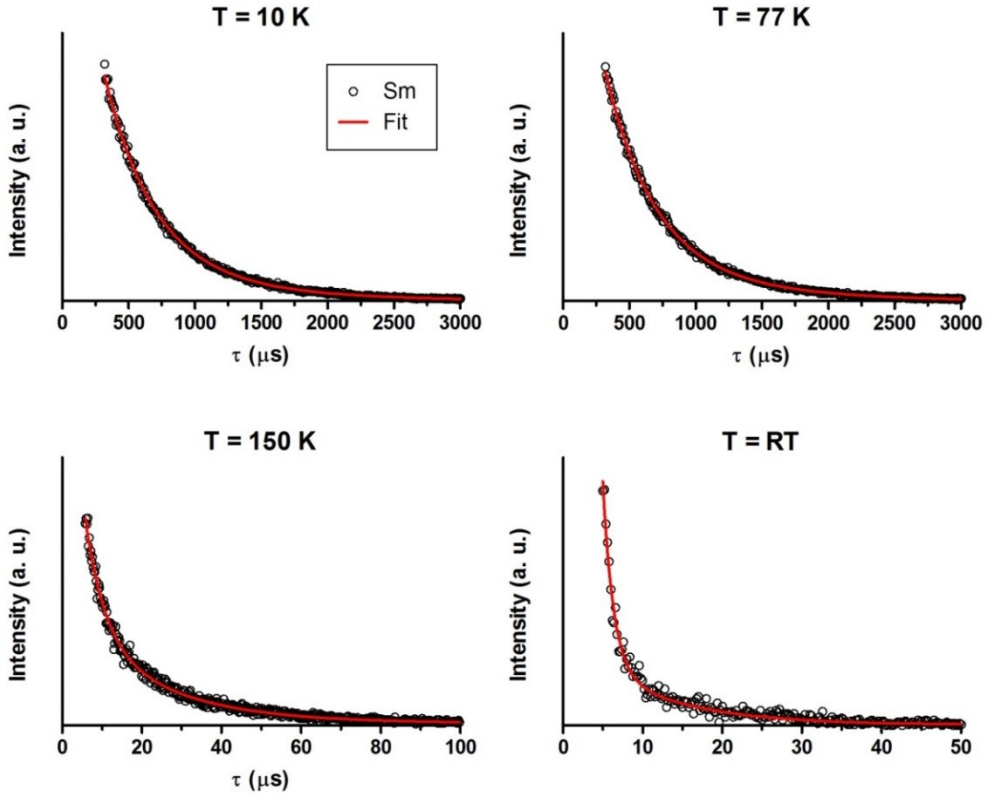

Figure S18.- Luminescence decay curves at different temperatures after excitation at 375 nm for Tb^{III} compound **6** monitored at 545 nm.

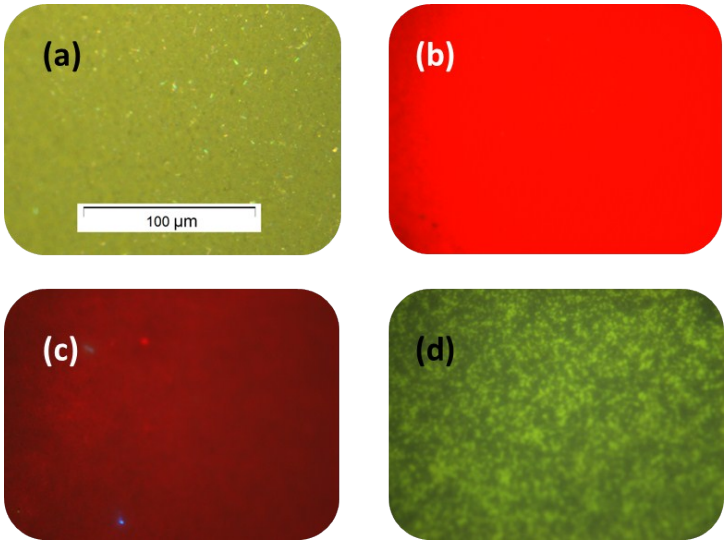

Figure S19.- Micro-photoluminescence images taken on powdered samples after irradiation with white light (reference) (a) and after excitation at 280 nm for Sm(III) (b), Eu(III) (c) and Tb(III) (d) derivatives at room temperature. All the images have been taken with the same scale.

Table S8.- Energy levels for complexes **6** and **11** calculated from luminescence and dc magnetic data.

Energy level complex **6** (cm^{-1})		Energy level complex **11** (cm^{-1})	
luminescence	Dc data	luminescence	Dc data
0	0	0	0
20	12	11	8
75	77	183	44
133	85	283	313
153	155		
190	215		
239	237		